# Cross-Correlation Between Polarization Channels in SAR Imagery Over Oceanographic Features

Camilla Brekke, *Member, IEEE,* Cathleen E. Jones, *Member, IEEE,* Stine Skrunes, *Member, IEEE,* Benjamin Holt, *Member, IEEE,* Martine Espeseth, and Torbjørn Eltoft, *Member, IEEE*

***Abstract*—This letter discusses cross-correlation features derived from near-coincident Radarsat-2 quad-polarimetric and RISAT-1 hybrid-polarity measurements collected during the Norwegian radar oil spill experiment in 2015 (NORSE2015). We show that the imaginary part of the cross-correlation between RH and RV is a hybrid-polarity parallel to the real part of the cross-correlation between HH and VV earlier proposed for oil spill charactarization. We compared the Radarsat-2 and RISAT-1 scenes, separated in time by less than an hour, and the results show a clear difference between the slicks across these acquisitions. The development of the oil spills were closely monitored during NORSE2015. Due to the evolving nature of the oil spills, and the weathering processes acting upon the spills, our results also indicate an importance of a high SAR sampling rate during an actual oil spill event.**

***Index Terms*—Synthetic aperture radar, hybrid-polarity, quad-polarimetry, cross-correlation features, oil spill.**

## I. Introduction

In recent years, multipolarization synthetic aperture radar (SAR) systems have been shown to be capable of characterizing oil spills in the marine environment, see, e.g., [1][2][3]. This development has potential value during a large scale oil spill incident as a tool for directing the mechanical and chemical response operations towards the thicker emulsions, i.e., parts of the slick with greater oil content, which can be characterized as a higher volumetric fraction of oil or greater thickness of oil. The oil spill characterization capability is also attractive for oil spill surveillance operations due to its potential in reducing false alarms on natural slicks (*look-alikes*).

However, there are still unanswered questions related to the polarization dependent electromagnetic signals and their relationship to oil-water mixtures' dielectric properties. The joint UiT The Arctic University of Norway and Jet Propulsion Laboratory (JPL)/National Aeronautics and Space Administration (NASA) NOrwegian Radar oil Spill Experiment (NORSE2015) was designed for systematic collection of X-, C-, and L-band SAR data over oil emulsions with known oil fraction and quantity. In addition, plant oil was released simulating a biogenic film. Auxiliary in-situ data, including meteorological and oceanographic observations and optical/infra-red imagery were also recorded.

C. Brekke, S. Skrunes, M. Espeseth, and T. Eltoft are with UiT The Arctic University of Norway, Postboks 6050 Langnes, 9037 Tromsø, Norway, Email:camilla.brekke@uit.no, stine.skrunes@uit.no, martine.espeseth@uit.no.

C. E. Jones and B. Holt are with Jet Propulsion Laboratory, California Institute of Technology, Pasadena, CA, USA, Email: cathleen.e.jones@jpl.nasa.gov, benjamin.m.holt@jpl.nasa.gov.

Manuscript received xxx xx, 201x; revised xxx xx, 201x.

This paper presents an initial study on near-coincident Radarsat-2 (RS-2) and Radar Imaging Satellite 1 (RISAT-1) SAR measurements collected during NORSE2015. The Indian RISAT-1 is an example of a hybrid-polarity (HP) SAR system [4], transmitting a right circular (R) polarized signal while receiving on two orthogonal mutually coherent linear polarized channels (V and H). RS-2 has a quad-polarimetric (QP) SAR capability (VV, HH, HV, and VH). The objective of this letter is to investigate features derived based on cross-correlation between polarization channels in the two different polarization systems, namely quad-polarimetry and HP.

Section II introduces NORSE2015 and gives a description of the dataset investigated in this study, which were the RS-2 QP SAR scene and the HP SAR product from RISAT-1 overlapping in time of acquisition and spatial coverage. The impact of additive noise is explored in section III. In a QP SAR system, there is a time delay between the acquisition of the HH and VV channels due to the interleaved transmit of H and V. When utilizing the real part of the copolarization cross-product as a mean for investigating the characteristics of oceanographic features [2], the coherence time of the target may therefore be critical. On the contrary, in a HP SAR system, the RH and RV channels are collected truly simultaneously. Section IV discusses the sensors pulse repetition frequency vs. the target decorrelation time. This discussion is followed by an investigation of cross-correlation features including a comparison between the sensors in section V. A counterpart for the real part of the copolarization cross-product is derived for the HP domain, and shown to have promising results. Finally, we give some concluding remarks in section VI.

## II. Norwegian radar oil spill experiment

Four experimental oil spills were released at the Frigg field in the North Sea in June 2015 ($59°59^{'}N, 2°27^{'}E$) during NORSE2015. The campaign was a collaboration between Norwegian Clean Seas Association for Operating Companies (NOFO), UiT and JPL/NASA, and involved various satellite acquisitions, e.g., RS-2, TerraSAR-X, and RISAT-1, acquisitions from Uninhabited Aerial Vehicle Synthetic Aperture Radar (UAVSAR) carried by a GulfStream-III, meteorological/ocean observations and photography of the slicks taken from the release vessel, and drift buoy and radiosonde releases.

Table I presents details about the experimental oil spills. The procedure of releasing the oils into the seawater started approximately at 04:50 UTC. The plant oil was released first and then followed by Emulsion 1 to 3 (E1 to E3). The release

TABLE I
DETAILS ABOUT THE EXPERIMENTAL OIL DISCHARGES.

| Release | Quantity | Specification |
|---|---|---|
| Emulsion 3 | 0.5 $m^3$ | 80 % oil and 20 % sea water (100 l). |
| Emulsion 2 | 0.5 $m^3$ | 200 l Troll, 200 l Oseberg, 0.2 l ONE-MUL. 60 % oil and 40 % water (200 l). |
| Emulsion 1 | 0.5 $m^3$ | 150 l Troll, 150 l Oseberg, 0.2 l ONE-MUL. 40 % oil and 60 % water (300 l). |
| Plant oil | 0.2 $m^3$ | 100 l Troll, 100 l Oseberg, 0.2 l ONE-MUL. 100 % oil: Radiagreen EBO. |

procedure finished at about 05:35 UTC. All four slicks were left untouched on the surface.

Table II presents the details of the SAR imagery applied in this study. Both the RISAT-1 and the RS-2 SAR systems

TABLE II
DETAILS ABOUT THE DATA SET APPLIED IN THIS STUDY.

| Sensor and mode | Time (UTC) | Polarisation | Coverage (rg × az) | Resolution (rg × az) |
|---|---|---|---|---|
| RS-2 FQ5W | 06:28 | HH, HV, VV and VH | 50 km × 25 km | 5.2 m × 7.6 m |
| RISAT-1 FRS-1 Hybrid | 07:19 | RH and RV | 25 km × 25 km | 2.2 m × 3 m |

operate at C-band frequencies. The incidence angle for RISAT-1 is approximately $44^\circ$ while the incidence angle range of the RS-2 scene covers $22.6^\circ - 26.0^\circ$. Note that the RS-2 QP SAR image was collected less than 1 hour earlier than the RISAT-1 HP image.

The slicks were aligned with the satellite overpass of RS-2 (and RISAT-1) along the azimuth direction, aiming for having the slicks lined up on approximately the same incidence angle. UAVSAR flights were later adapted to fit this configuration. The four slicks were released with a spacing of approximately 0.5 nautical miles. The arrangement of the experimental slicks is shown in detail in Fig. 1. In both the RS-2 and the RISAT-1 scenes, the four slicks are located close to mid swath. This was done on purpose for RS-2 to exploit the minimum noise floor level at mid swath incidence angle, and hence increase the signal-to-noise level over the slicks.

A discussion of the additive noise in RS-2 is given next.

## III. NOISE ANALYSIS

In a full polarimetric SAR system such as RS-2, the HV and VH channels are measured independently. As additive noise increases, the correlation coefficient between HV and VH decreases from the limiting case of 1 in the absence of noise ([5], and references therein). Accordingly, Fig. 2 shows that the noise level over clean sea water increases at the near and far range of the radar swath.

Fig. 3 presents a noise analysis, adopting the methodology described in [5], [6]. For the RS-2 scene, the eigenvalue-eigenvector decomposition analysis of the coherence matrix $[T_4]$ revealed that $\lambda_4 > 0$, which can be used to derive the noise level of the data [5]. Fig. 3 (a) presents the intensity image of the HV polarization channel, with a clear intensity

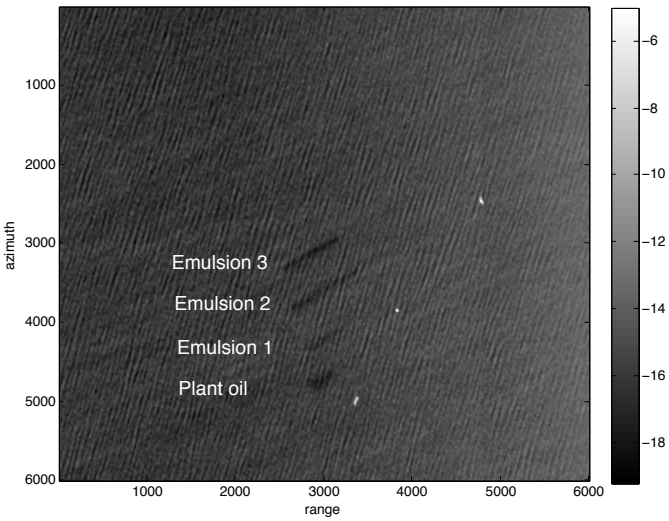


Fig. 1. Subsection (6000 × 6000 pixels) of RISAT-1 scene (pixel spacing: 2.3 m). Intensity RV image on log-scale. All four slicks and three ships are visible. RISAT-1 ©2015-Antrix, processed by KSAT, all rights reserved 2015.

variation across the swath. An analysis of the eigenvalues confirms that a transect through $\lambda_4$ reflects the variation in noise floor across range (Fig. 3 (b)). By subtracting $\lambda_4$ from $\lambda_1$, $\lambda_2$, and $\lambda_3$ and reconstructing a new coherency matrix we can obtain a noise corrected intensity image of the HV channel. The four slicks are now more easily seen mid swath in the upper part of the image (Fig. 3 (c)). An elongated larger slick is also noticed below this region which is remains from an oil spill exercise the day before. From our analysis, the benefit of releasing the four experimental slicks mid swath is clear. The signal across the four slicks are also confirmed, but not shown here, to lie well above the noise floor in VV and HH polarization (mean backscatter values about 27-29 dB above the Noise-Equivalent Sigma Zero).

Next, we justify the applicability of QP cross-correlation features based on an analysis of the ocean decorrelation time.

## IV. PRF AND TARGET DECORRELATION TIME

For RS-2 Fine Q5 Wide QP SAR mode, the pulse repetition frequency (PRF) is 2671 Hz. This corresponds to a pulse repetition interval (PRI) of 0.000374 s. RISAT-1 FRS-1 operates at a PRF of 2948 Hz, which corresponds to a PRI of 0.000339 s. It is of interest to get an estimate of the decorrelation time $\tau_c$ of the individual facets within the resolution cell of the SAR system. From the literature, open water is reported to decorrelate in less than 0.05 s at C-band and between 0.05 - 0.1 s for L-band ([7], and references therein). These references are often cited, but some of them point to the TOWARD campaign from the 1980s conducted under specific environmental conditions; wind speeds $\leq$ 8 m/s, and a significant wave height of $<=$ 1.6 m [8]. However, during our experiment the environmental conditions were slightly rougher with wind speeds of 9-12 m/s and a wave height 2-2.5 m. We therefore refer to Milman et al. [9] who derived an expression for $\tau_c$ for a range of different wind speeds and radar wavelengths. For convenience we reproduce

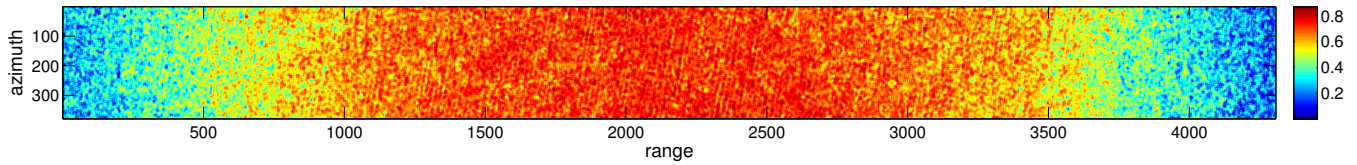


Fig. 2. Subsection (4328 × 400 pixels) of RS-2 scene (pixel spacing: 4.7 m) over a clean sea only: correlation coefficient, HV and VH, using ensemble averaging of 11 × 11.

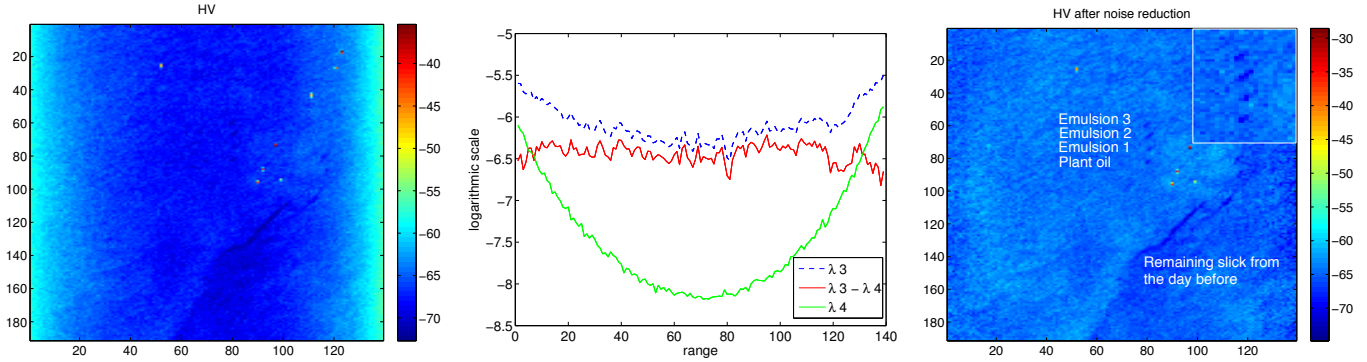


(a) (b) (c)

Fig. 3. Eigenvalue-based noise analysis of RS-2. (a) HV-polarization channel (intensity, dB-scale), (b) eigenvalue transects (through E2) along range direction, and (c) noise reduced HV-polarization channel (intensity, dB-scale). Zoom-in on oil slicks overlaid in upper right corner.

the most relevant values in Table III. In summary, we find

TABLE III
DECORRELATION TIMES FOR C-BAND AND $\theta = 30°$. ADAPTED FROM [9].

| Windspeed | 5 m/s | 10 m/s | 15 m/s |
|---|---|---|---|
| $\tau_c$ | 0.1 | 0.052 | 0.034 |

that the PRI of RS-2, which clearly is orders of magnitude smaller than $\tau_c$, should be sufficient to provide correlated VV and HH channels over ocean under the higher wind conditions experienced during our campaign.

We proceed with a discussion on cross-correlation features.

## V. CROSS-CORRELATION FEATURES

Previously, the real part of the copolarization cross-product was identified as a powerful multipolarization SAR feature for mineral vs. simulated biogenic slick discrimination [2]. The real part of the copolarization cross-product is defined as:

$$r_{co} = |\Re(\langle S_{HH} \cdot S_{VV}^* \rangle)|, \tag{1}$$

where $\Re(\cdot)$ represents the real part and $|\cdot|$ the absolute value. A difference in the correlation over clean ocean as compared to over an oil slick has previously been explained by a difference in scattering mechanism, i.e., non-Bragg scattering in slick-covered areas vs. Bragg-type scattering in clean sea and look-alikes [10]. However, a description of an alternative scattering mechanism is lacking in the literature, urging further investigations. Note that other studies have reported Bragg scattering to be consistent across both oil and water, see, e.g., [1], suggesting caution in the interpretation.

### A. RISAT-1

With its circular transmit signal and simultaneous dual-channel polarization reception, all the scattering coefficients of the HP scattering matrix are collected simultaneously. The scattering matrix, for a right circular transmitting (CT) and linear receiving (LR for a H and V) system, is given as

$$\begin{aligned} C_{CTLR} &= \langle \vec{k}_{CTLR} \cdot \vec{k}_{CTLR}^{*T} \rangle \\ &= \begin{bmatrix} \langle |S_{RH}|^2 \rangle & \langle S_{RH} \cdot S_{RV}^* \rangle \\ \langle S_{RV} \cdot S_{RH}^* \rangle & \langle |S_{RV}|^2 \rangle \end{bmatrix} \end{aligned} \tag{2}$$

where $\langle \cdot \rangle$ represents spatial averaging, $*$ is the complex conjugate, and $T$ the transpose operator. The scattering vector is defined as

$$\begin{aligned} \vec{k}_{CTLR} = \begin{bmatrix} S_{RH} \\ S_{RV} \end{bmatrix} &= \frac{1}{\sqrt{2}} \begin{bmatrix} S_{HH} & S_{VH} \\ S_{HV} & S_{VV} \end{bmatrix} \begin{bmatrix} 1 \\ -j \end{bmatrix} \\ &= \frac{1}{\sqrt{2}} \begin{bmatrix} S_{HH} - jS_{HV} \\ S_{VH} - jS_{VV} \end{bmatrix} \end{aligned} \tag{3}$$

where $j$ represents the imaginary unit.

We identify a counterpart to $r_{co}$ in the HP domain. From eq. 2, we have that $C_{CTLR}^{12} = \langle S_{RH} \cdot S_{RV}^* \rangle$. By assuming reciprocity ($S_{HV} = S_{VH}$), we can express $\Im(C_{CTLR}^{12})$ as

$$\begin{aligned} \Im(\langle S_{RH} \cdot S_{RV}^* \rangle) = \frac{1}{2} (&\Re(\langle S_{HH} \cdot S_{VV}^* \rangle) \\ &- \langle |S_{HV}|^2 \rangle \\ &+ \Im(\langle S_{HH} \cdot S_{HV}^* \rangle + \langle S_{HV} \cdot S_{VV}^* \rangle)). \end{aligned} \tag{4}$$

In Fig. 4, both $\langle |S_{HV}|^2 \rangle$ and $|\Im(\langle S_{HH} \cdot S_{HV}^* \rangle + \langle S_{HV} \cdot S_{VV}^* \rangle)|$ (see also [11]) are shown to be much smaller than $\Re(\langle S_{HH} \cdot S_{VV}^* \rangle)$. In view of this, we assume the following approximation:

$$2\Im(\langle S_{RH} \cdot S_{RV}^* \rangle) \approx \Re(\langle S_{HH} \cdot S_{VV}^* \rangle). \tag{5}$$

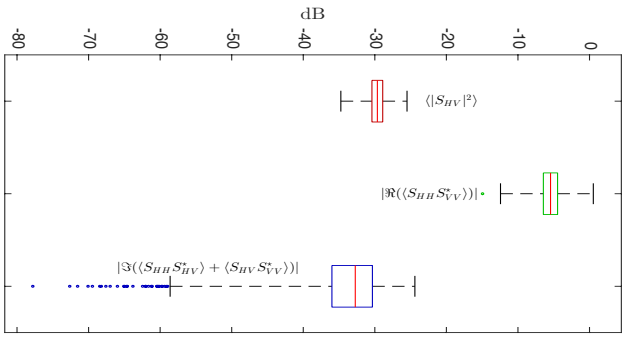


Fig. 4. Box plot showing the components of eq. 4. The central mark within each box is the median. The edges of the boxes are the 25th and 75th percentiles. The outliers (dots) extend to the most extreme data.

Hence, in the HP domain, we can treat

$$\bar{i}_{co} = |\Im(\langle S_{RH} \cdot S_{RV}^* \rangle)| \tag{6}$$

as a proxy for $r_{co}$.

In addition, it is natural to study several related CTLR cross-correlation parameters, all defined in Table IV. These CTLR

TABLE IV
CTLR PARAMETERS AS DEFINED IN THIS WORK.

| Feature | Definition |
|---|---|
| $\overline{co}$ | $\lvert\langle S_{RH} \cdot S_{RV}^* \rangle\rvert$ |
| $\bar{r}_{co}$ | $\lvert\Re(\langle S_{RH} \cdot S_{RV}^* \rangle)\rvert$ |
| $\bar{i}_{co}$ | $\lvert\Im(\langle S_{RH} \cdot S_{RV}^* \rangle)\rvert$ |
| $\bar{\rho}$ | $\left\lvert \frac{\langle S_{RH} \cdot S_{RV}^* \rangle}{\sqrt{\langle\lvert S_{RH}\rvert^2\rangle \cdot \langle\lvert S_{RV}\rvert^2\rangle}} \right\rvert$ |

cross-correlation parameters are here compared with respect to i) the empirically observed contrast between the slicks and the surrounding sea, and ii) the Pearson population correlation coefficient between the most powerful features.

Fig. 5 shows $\bar{r}_{co}$, $\bar{i}_{co}$, and $\bar{co}$, respectively, on a linear scale. The correlation coefficient between RH and RV, $\bar{\rho}$, is not shown because the contrast was found to be considerably lower between the slicks and the ocean in this case; the four slicks were only barely visible. A plausible explanation for this could be that the normalization reduces the radiometric information across the scene [2]. What is noticable in Fig. 5 is a difference in slick-to-sea contrast between (a) and (b)-(c). $\overline{co}$ has the largest dynamic range $[0, 0.0298]$, followed closely by $\bar{i}_{co}$ $[0, 0.0283]$ and then $\bar{r}_{co}$ $[0, 0.0138]$.

Looking at the correlation between pairs of the features in Table V, we see that $\overline{co}$ and $\bar{i}_{co}$ are strongly correlated, while the correlation between $\bar{r}_{co}$ and any of the other features reduces the score. This corresponds to the visual impression we get from Fig. 5.

Based on the $\bar{i}_{co}$ parameter, there are differences visible in the shape and structure of the four slicks. In the following subsection, we compare this feature with $r_{co}$ derived from the QP RS-2 measurements.

TABLE V
LINEAR DEPENDENCE BETWEEN PAIRS OF CTLR PARAMETERS. SAMPLES ARE COLLECTED ALONG A TRANSECT THROUGH ALL SLICKS (LINE 800 ON X-AXIS OF FIG. 5). $R$: PEARSON CORRELATION COEFFICIENT.

| Feature | $R$ |
|---|---|
| $\overline{co}$ vs. $\bar{i}_{co}$ | 0.9912 |
| $\overline{co}$ vs. $\bar{r}_{co}$ | 0.7791 |
| $\bar{i}_{co}$ vs. $\bar{r}_{co}$ | 0.6915 |

### B. Comparing RS-2 and RISAT-1

Fig. 6 shows $r_{co}$ for RS-2 on a linear scale. As expected, and similar to $\bar{i}_{co}$ (panel (b) of Fig. 5), the slicks exhibit lower feature values as compared to the surrounding sea. The separation between the slicks and the ambient sea water is visually enhanced with increased smoothing in Fig. 6. However, there are still clear differences between the four slicks in all panels.

For $\bar{i}_{co}$ (panel (b) of Fig. 5), E1 has the lowest contrast to the surrounding sea as compared to E2 followed by E3. This can probably be explained by the relative increasing oil content of the slicks from E1 to E3 (see Table I).

In Fig. 6, however, E2 is the most pronounced while E1 is the least pronounced among the mineral slicks. This could possibly be explained by the shorter time E3 has been on the surface in RS-2 (slightly less than 1 hour) than E2 (about 75 minutes) and E1 (about 90 minutes). It is likely that E3 is still developing and has not yet reached its maximum extent at the time of the RS-2 acquisition (06:28 UTC).

During NORSE2015, the wind speed was ∼9-12 m/s and the wave height was ∼2-2.5 m. Despite the more pronounced wave pattern in RISAT-1, the plant oil slick has a clearer signature in $\bar{i}_{co}$ as compared to $r_{co}$ (RS-2). The improved resolution of RISAT-1 over RS-2 is likely to be an advantage. Empirical evidence also shows that the incidence angle has an impact on the feature values. However, a comparison of the plant oil spill with the emulsions deserves its own study, and is not pursued further here.

In summary, due to the evolving nature of the spills and the weathering processes acting upon the releases, these results emphasize the importance of a high SAR image sampling rate during an actual oil spill event.

## VI. CONCLUDING REMARKS

We present the first results on cross-correlation features derived from near-coincident RS-2 QP and RISAT-1 HP measurements collected during NORSE2015.

The real part of the copolarization cross-product has previously been reported as a powerful descriptor with potential in characterizing mineral and biogenic slicks on ocean. This paper contributes to the field by a thorough discussion of the coherence time of the target vs. the PRI of the SAR modes investigated, arguing that the PRI of RS-2 is sufficient to provide correlated VV and HH channels over oceanographic features.

We have shown that the imaginary part of the cross-correlation between RH and RV is a HP parallel to the real part

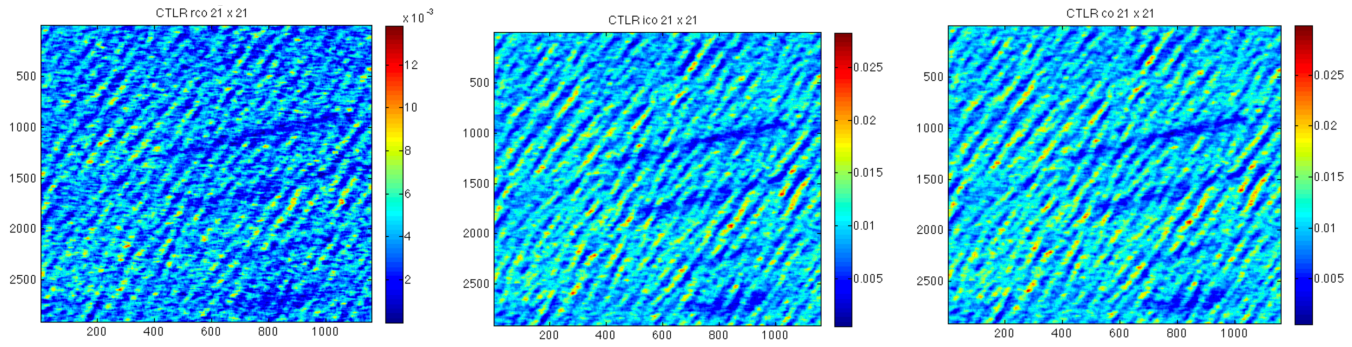


(a) (b) (c)

Fig. 5. A subscene of the RISAT-1 image containing all four oil spills. $\bar{r}_{co}$ , $\bar{i}_{co}$, and $\overline{co}$ are shown using an ensemble averaging of $21 \times 21$ pixels.

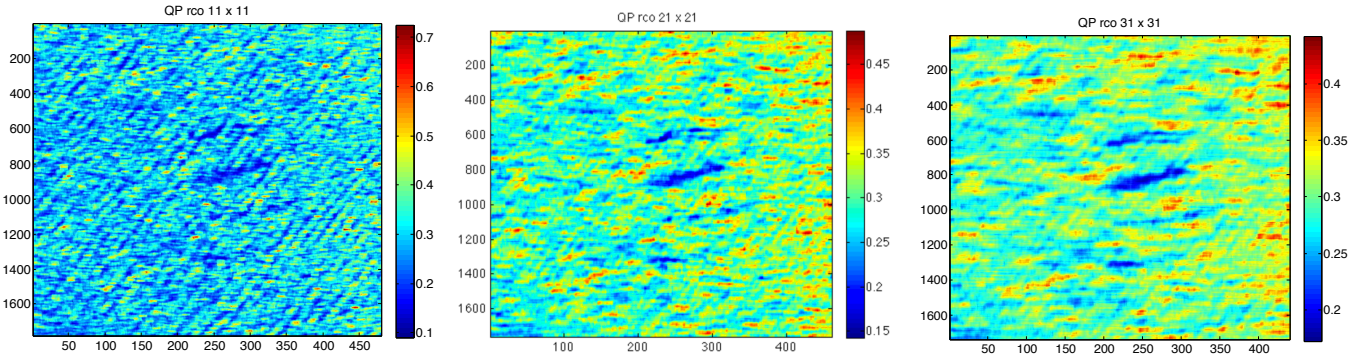


(a) (b) (c)

Fig. 6. A subscene of the RS-2 image containing all four oil spills. $r_{co}$ using an ensemble averaging of $11 \times 11$, $21 \times 21$, and $31 \times 31$ pixels.

of the cross-correlation between HH and VV, and empirically it exhibits a comparable performance to the magnitude of the cross-product between RH and RV.

Last, we compared the RS-2 and the RISAT-1 scenes separated in time by less than an hour. The results show a clear difference between the slicks across the acquisitions. Aiming at increased understanding of SAR characteristics distinguishing monomolecular biogenic slicks and thicker mineral oil emulsions, our future work will cover an investigation of a time series of 22 QP UAVSAR images collected over a period of eight hours following the release of the four slicks under NORSE2015.

## ACKNOWLEDGMENT

This research was carried out in part at the Jet Propulsion Laboratory, California Institute of Technology, under contract with the National Aeronautics and Space Administration. RS-2 data was provided by NSC/KSAT, Norwegian-Canadian Radarsat agreement 2015. RISAT-1 data was provided through GlobOilRisk (RCN project no. 235444). NORSE2015 was partly financed by CIRFA (RCN grant no. 237906). Thanks to MET Norway for collecting met/ocean observations, NOFO for hosting NORSE2015, and colleague Thomas Kræmer for discussions.

## REFERENCES

[1] Minchew, B., Jones, C. E., and Holt, B., *"Polarimetric Analysis of Backscatter From the Deepwater Horizon Oil Spill Using L-Band Synthetic Aperture Radar"*, IEEE Trans. Geosci. Remote Sens., vol. 50, no. 10, pp. 3812-3830, Oct. 2012.

[2] Skrunes, S., Brekke, C., and Eltoft, T., *"Characterization of Marine Surface Slicks by Radarsat-2 Multipolarization Features"*, IEEE Trans. Geosci. Remote Sens., vol. 52, no. 9, pp. 5302-5319, Sept. 2014.

[3] Skrunes, S., Brekke, C., Eltoft, T., and Kudryavtsev, V., *"Comparing Near-Coincident C- and X-Band SAR Acquisitions of Marine Oil Spills"*, IEEE Trans. Geosci. Remote Sens., vol. 53,no. 4, pp. 1958-1975, April 2015.

[4] Raney, R. K., *"Hybrid-Polarity SAR Architecture"*, IEEE Trans. Geosci. Remote Sens., vol 45, no. 11, pp. 3397-3404, Nov. 2007.

[5] Hajnsek, I., Pottier, E., and Cloude, S. R., *"Inversion of Surface Parameters From Polarimetric SAR"*, IEEE Trans. Geosci. Remote Sens., vol. 41, no. 4, April 2003.

[6] Angelliaume, S., Dubois-Fernandez, P., Miegebielle, V., and Dubucq, D., *"Polarimetric Parameters for Oil Slicks Detection Using SAR Data Remote Sensing - An Evaluation"*, In Proc. IGARSS, Milan, Italy, pp. 3794-3797, 2015.

[7] Ouchi, K. and Wang, H., *"Interlook cross-correlation function of speckle in SAR images of sea surface processed with partially overlapped subapertures"*, IEEE Trans. Geosci. Remote Sens., vol. 1, no. 3, pp. 184-187, July 2004.

[8] Shemdin, O. H., *"Tower Ocean Wave and Radar Dependence Experiment: An Overview"*, Journal of Geophysical Reserach, vol. 93, no. C11, pp. 13829-13836, 15 Nov., 1988.

[9] Milman, A. S., Scheffler, A. O., and Bennett, J. R., *"A Theory of the Synthetic Aperture Radar Images of Time-Dependent Scenes"*, Journal of Geophysical Research, vol. 98, no. C1, pp. 911-925, 15 Jan., 1993.

[10] Migliaccio, M., Gambardella, A., Nunziata, F., Shimada, M., and Isoguchi, O., *"The PALSAR polarimetric mode for sea oil slick observation"*, IEEE Trans. Geosci. Remote Sens., vol. 47, no. 12, pp. 4032-4041, Dec. 2009.

[11] Nghiem, S. V., Yueh, S. H., Kwok, R., and Li, F. K., *"Symmetry properties in polarimetric remote sensing"*, Radio Sci., vol. 27, no. 5, pp. 693-711, Sep.-Oct. 1992.